International Journal of Pharmaceutics: X 8 (2024) 100291

Contents lists available at ScienceDirect

International Journal of Pharmaceutics: X

journal homepage: www.sciencedirect.com/journal/international-journal-of-pharmaceutics-x

Multifunctional poloxamer-based thermo-responsive hydrogel loaded with human lactoferricin niosomes: *In vitro* study on anti-bacterial activity, accelerate wound healing, and anti-inflammation

Sirikwan Sangboonruang [a,b], Natthawat Semakul [c], Kiattikhun Manokruang [c,d], Nuttawut Khammata [c], Kanyaluck Jantakee [e], Katanchalee Mai-Ngam [f], Satrawut Charoenla [f], Phadungkiat Khamnoi [g], Kanokwan Saengsawang [h], Usanee Wattananandkul [a], Sorasak Intorasoot [a], Khajornsak Tragoolpua [a,*]

[a] *Division of Clinical Microbiology, Department of Medical Technology, Faculty of Associated Medical Sciences, Chiang Mai University, Chiang Mai 50200, Thailand*
[b] *Office of Research Administration, Chiang Mai University, Chiang Mai 50200, Thailand*
[c] *Department of Chemistry, Faculty of Science, Chiang Mai University, Chiang Mai 50200, Thailand*
[d] *Center of Excellence in Materials Science and Technology, Chiang Mai University, Chiang Mai 50200, Thailand*
[e] *Department of Biology, Faculty of Science, Chiang Mai University, Chiang Mai 50200, Thailand*
[f] *National Metal and Materials Technology Center, National Science and Technology Development Agency, Pathumthani 12120, Thailand*
[g] *Diagnostic Laboratory, Maharaj Nakorn Chiang Mai Hospital, Faculty of Medicine, Chiang Mai University, Chiang Mai 50200, Thailand*
[h] *Department of Medical Technology, Lampang Hospital, Lampang 52000, Thailand*

ARTICLE INFO

Keywords:
Lfcin-Nio
Thermo-responsive hydrogel
Anti-bacterial activity
Wound healing
Anti-inflammation

ABSTRACT

Chronic wound infections are attributed to delayed tissue repair, which remains a major clinical challenge in long-term health care. Particularly, infections with antibiotic resistance have more serious effects on health, often resulting in unsuccessful treatments. Thus, antimicrobial peptide (AMP)-based therapy holds promise as a potential therapeutic approach to overcoming drug resistance. Conventional wound dressing is a passive strategy for wound care that is not capable of eradicating pathogens and promoting tissue repair. In this study, we aim to construct an advanced wound dressing; a thermo-responsive hydrogel incorporated with lactoferricin (Lfcin) niosome (Lfcin-Nio/hydrogel) for bacterial pathogen treatment. The Lfcin-loaded niosome (Lfcin-Nio) has a particle size of 396.91 ± 20.96 nm, 0.38 ± 0.01 of PdI, −10.5 ± 0.3 mV of ζ potential, and 72.30 ± 7.05 % Lfcin entrapment efficiency. Lfcin-Nio exhibited broad antibacterial activity on both drug-susceptible and drug-resistant strains, and also on bacteria residing in the biofilm matrix. The Lfcin-Nio/hydrogel was fabricated from 0.5 % *w/v* poloxamer 188–20 % w/v poloxamer 407, and supplemented with Lfcin-Nio and epidermal growth factor (EGF). The physical properties of Lfcin-Nio/hydrogels showed elasticity, swelling ability, and strong injectability with responsiveness to 33–37 °C temperatures. The biological properties of Lfcin-Nio/hydrogels exhibited a bactericidal effect against drug-resistant strains of *S. aureus* and *P. aeruginosa,* and showed less toxicity to the human skin fibroblast. It also promoted the healing of scratches by 55 % within 6 h, compared to the wound closure rate of 20 % in the cell control. The inflammatory response of the Lfcin-Nio/hydrogel-treated cells was reduced *via* suppression of *IL-1β* and *COX-2* mRNA expressions. From this study,

Abbreviations: AMP, Antimicrobial peptide; Lfcin, Human lactoferricin 1–11; NP, Nanoparticle; Nio, Niosome; PEO, Polyethylene oxide; PPO, Polypropylene oxide; P407, Poloxamer 407; P188, Poloxamer 188; EGF, Epidermal growth factor; ATCC, American type culture collection; MRSA, Methicillin-resistant *S. aureus*; VISA, Vancomycin-intermediated *S. aureus*; ESBL, Extended-spectrum β-lactamase; CCD-1123Sk, human skin fibroblast; TFH, Thin-film hydration; DLS, Dynamic light scattering; PDI, Polydispersity index; ZP, Zeta potential; EE, Entrapment efficiency; CFU, Colony-forming unit; MBC, Minimum bactericidal concentration; VAN, Vancomycin; Mpm, Meropenem; sol, Solutions; gel, Hydrogel; G', Storage modulus; G", Loss modulus; LVR, Linear viscoelastic region; LPS, Lipopolysaccharide; IL-1β, Interleukin-1 beta; TGF-β, Transforming growth factor beta; COX-2, Cyclooxygenase-2; GAPDH, glyceraldehyde-3-phosphate dehydrogenase; EPS, Extracellular polymeric substance.

* Corresponding author.
E-mail address: khajornsak.tr@cmu.ac.th (K. Tragoolpua).

https://doi.org/10.1016/j.ijpx.2024.100291
Received 9 July 2024; Received in revised form 9 October 2024; Accepted 9 October 2024
Available online 11 October 2024

Lfcin-Nio/hydrogels can be suggested as a modern wound dressing that possesses multifunctional and beneficial properties for the management of chronic wound infections.

1. Introduction

Bacterial infection is a serious complication of chronic wounds that can often lead to delayed or non-healing wounds and high rates of amputation (Zhou et al., 2022). Thus, reducing the bacterial burden in wounds is a critical part of treatment, and antibiotic therapy is required. However, overprescribing or the indiscriminate use of antibiotics may increase the risk of side effects and the development of antibiotic resistance (Falcone et al., 2021). In addition, prolonged courses of antibiotics may hamper wound repair (Monika et al., 2021). Due to the rise of bacterial resistance in conventional antibiotics, antimicrobial peptide (AMP)-based therapeutics have drawn the attention of complementary and alternative therapies for traumatic infections (Ding et al., 2022).

Human lactoferricin 1–11 (Lfcin) is a small AMP derived from the iron-binding glycoprotein lactoferrin (Lf) through pepsin cleavage. It is a potential candidate against a wide spectrum of pathogens, such as viruses, fungi, and bacteria, including antibiotic-resistant bacteria (Intorasoot et al., 2022), through an interaction between the positively charged region of AMPs and the negatively charged surfaces of microorganisms (Ohradanova-Repic et al., 2023). Several previous studies have demonstrated its anti-microbial abilities to be greater than Lf (Fernandes and Carter, 2017; Vega Chaparro et al., 2018). Moreover, Lf exhibits non-hemolytic activity (Intorasoot et al., 2022) that ensures safety for invasive wound management. However, short peptides might have limited stability within the host and in microbial proteolytic enzyme conditions (Kapil and Sharma, 2021; Intorasoot et al., 2022). Hence, nanoencapsulation is regarded as an effective approach to improve its therapeutic efficacy.

Nanoencapsulation is the encapsulation of a therapeutic compound into a nanoparticle (NP) that offers protection of the payload from degradation or clearance, as well as sustained-release treatment on a therapeutic level. NPs exist in different platforms, such as polymeric NPs and lipid-based vesicles. Among these, lipid-based nanovesicles such as liposomes and niosomes provide more advantages and are widely used in topical drug delivery systems (Muzzalupo et al., 2011). Several previous studies have performed Lf encapsulation using different nanoplatforms, as well as liposomes, and their abilities against many microorganisms have been described (Lopez-Machado et al., 2021; Ong et al., 2023). However, Lfcin-nanoencapsulation has not been mentioned.

In topical medication for chronic wounds, traditional dressings such as gauze, cotton pads, and bandages are still lacking in support for wound repair and bacterial elimination (Powers et al., 2016; Zhang et al., 2020). Hence, hydrogel-based modern wound care has become a better option. Hydrogels have crosslinked, polymeric, three-dimensional (3D) structure networks composed of hydrophilic substances with high water absorption abilities. Owing to their excellent moisturizing ability, hydrogels are practical wound dressings that provide a moist environment for wounds and absorb tissue exudates (Shi et al., 2020; Serpico et al., 2023). Furthermore, hydrogels are able to contain drugs and several active substances to eradicate various pathogens and accelerate the wound-healing process. In recent years, poloxamer-based hydrogels have been extensively studied as a smart material in biomedicines. Poloxamers are triblock copolymers composed of polyethylene oxide (PEO) and polypropylene oxide (PPO), and are widely used to fabricate stimuli-responsive, drug-loaded hydrogels that respond to the external environment, which includes reactive oxygen species (ROS), pH, glucose, enzymes, and temperature (Pourjavadi et al., 2021). Thus, the development of a multifunctional and shape-adaptable wound dressing based on a poloxamer hydrogel could provide greater advantages.

In this study, we designed an injectable, thermo-responsive hydrogel incorporated with epidermal growth factor (EGF) and Lfcin-Nio for the treatment of chronic wound infections. The Lfcin-Nio was fabricated and investigated for its physicochemical properties. The antimicrobial activity of the NPs was evaluated on the reference bacterial strains, and the clinical strains were isolated from the pus specimens. The hydrogels were constructed using poloxamer 407 (P407) and poloxamer 188 (P188), and were uniformly dispersed with EGF and Lfcin-Nio. The NP-loaded hydrogels were then evaluated for many properties, such as rheology and biological activities, including anti-bacterial activity, cytotoxicity, wound healing ability, and anti-inflammatory activity. Hence, this multifunctional hydrogel-based dressing may offer many of the required properties for chronic wound care and could potentially serve as the new generation of wound dressings.

2. Materials and methods

2.1. Materials

D-form of hLfcin 1–11 (GRRRRSVQWCA) was previously generated (Intorasoot et al., 2022) and synthesized by Synpeptide (Synpeptide Co., Ltd., Shanghai, China) and prepared in a 10 mg/mL stock concentration. Vancomycin was purchased from Sigma-Aldrich (Sigma-Aldrich, MO, USA). Meropenem (Monem, Biolab CO., Ltd., Bangkok, Thailand) was kindly gifted from Asst. Prof. Kulwadee Phannachet, Department of Microbiology, Faculty of Medicine, Chiang Mai University. The epidermal growth factor (EGF) was obtained from the National Metal and Materials Technology Center, National Science and Technology Development Agency (NSTDA), Thailand. Sorbitan monostearate (Span 60), polysorbate (Tween 80), cholesterol (CHOL), poloxamer 407 (P407), and poloxamer 188 (P188) were purchased from Sigma-Aldrich (Sigma-Aldrich, MO, USA). All other chemicals used were of analytical grade.

2.2. Bacterial strains

The bacterial strains used in this study were *Staphylococcus aureus* ATCC25923, *Pseudomonas aeruginosa* ATCC27853, *Klebsiella pneumoniae* ATCC700603, and *Escherichia coli* ATCC25922, and clinical isolates from pus. The *S. aureus*, *P. aeruginosa*, *K. pneumoniae*, and *E. coli* were obtained from the Clinical Microbiology Service Unit (CMSU), Faculty of Associated Medical Sciences, Chiang Mai University. The multidrug-resistant *P. aeruginosa* and methicillin-resistant *S. aureus* (MRSA) were obtained from the Clinical Microbiology Laboratory, Maharaj Nakorn Chiang Mai Hospital, and further identified for vancomycin-intermediated *S. aureus* (VISA) using a vancomycin agar screening method according to the Clinical Laboratory Standards Institute (CLSI) guidelines (M07-A9 and M100S-S22). The extended-spectrum β-lactamase (ESBL) strains include *K. pneumoniae* and *E. coli* were obtained from Lampang Hospital.

2.3. Cell culture

The human skin fibroblast (CCD-1123Sk) cell line (kindly obtained from Assoc. Prof. Dr. Chalermchai Pilapong, Department of Radiologic Technology, Faculty of Associated Medical Sciences, Chiang Mai University, Chiang Mai, Thailand) was cultured in Dulbecco's modified Eagle's medium (DMEM) (Gibco, NY, USA), supplemented with 10 % (*v*/v) fetal bovine serum (FBS), penicillin (100 units/mL) and streptomycin (100 μg/mL), and were maintained in a humidified atmosphere of 5 % CO_2 at 37 °C.

2.4. Formulation of Lfcin-Nio by thin-film hydration method

Niosome formulations were prepared according to the thin-film hydration (TFH) method according to previous work, (Sangboonruang et al., 2021) with some modifications. Briefly, the surfactants (span 60 and tween 80) and cholesterol were dissolved in 5 mL chloroform in a round bottom flask. The organic solvent was evaporated using a rotary evaporator under a vacuum at 50 °C, 100 rpm to produce a thin lipid film. The thin film was then hydrated with 5 mL PBS (pH 7.4) containing Lfcin (Lfcin-Nio) at 50 °C under mechanical stirring. The formulation without Lfcin was also prepared as an empty-niosome (Nio). The resulting niosome dispersion was sonicated for size reduction using an ultrasonic probe homogenizer (Hielscher UP50H, Hielscher Ultrasonics GmbH, Teltow, Germany) at 80 % amplitude for 30 min in an ice bath.

2.5. Physicochemical characterization of Lfcin-Nio

2.5.1. Particle size, polydispersity index (PDI), and surface charge analysis

The average particle size, PDI, and ζ-potential (ZP) of surface charge of the niosome formulations were determined using a dynamic light scattering (DLS) Zetasizer by Zetasizer Nano ZSP system (Malvern Instruments, Malvern, UK). The measurements were taken for empty-Nio and Lfcin-Nio formulations in an aqueous medium at a 1/100 dilution. Each sample was measured based on at least three measurements in three individual trials.

2.5.2. Morphology

The morphological characteristics of the optimized formula of the nano-formulations were observed by scanning transmission electron microscopy (STEM) with JSM-IT800 Ultrahigh Resolution Field Emission SEM (JEOL, Tokyo, Japan). A drop of niosome sample was deposited on a carbon-coated copper grid surface, then negatively stained with a 1 % phosphotungstic acid solution. The samples were dried at room temperature before visualization.

2.5.3. Entrapment efficiency (EE)

Free Lfcin was separated from Lfcin-Nio by ultracentrifugation with a 10 kDa molecular weight cut-off of 8000 ×g at 4 °C for 6 h. The niosomal pellets were re-suspended in 1 mL of PBS. The filtrates were collected to determine the free Lfcin using a UV–Vis spectrophotometer at 280 nm. The amount of loaded Lfcin was obtained by subtracting the amount of free drug from the total drug incorporated in a 5 mL niosomal dispersion. The following equation was used to determine the EE of Lfcin in niosomes:

$$\%EE = [\text{Lfcin used in preparation} - \text{Lfcin in supernatant}] / \text{Lfcin used in preparation} \times 100$$

2.5.4. Fourier transform infrared (FT-IR) spectrometry

To ensure that Lfcin-Nio was successfully prepared, the functional group of chemical substances in the formulations was studied by infrared spectroscopy. Lfcin, empty-Nio, and Lfcin-Nio samples were lyophilized prior to analysis. FT-IR spectra were recorded in the range of 4000–400 cm^{-1} at a resolution of 2 cm^{-1} using the attenuated total reflectance (ATR) mode of the FT-IR spectrometer (Bruker Tensor 27, Bremen, Germany).

2.6. In vitro drug release

A drug release assay was performed to assess the amount of Lfcin released from the niosomes in PBS, and was adjusted to pH 5.5 and 7.4 using a dialysis membrane with a molecular weight cut-off of 3.5 kDa (D-Tube™ Dialyzer Midi, Merck, Darmstadt, Germany). A sample of Lfcin-Nio (800 µL) was dialyzed against 50 mL of PBS at 37 °C. At specific time intervals (0, 1, 2, 3, 4, 6, 12, 24, and 48 h), 3 mL of PBS was collected and replaced with the same volume of fresh buffer. The buffer samples were analyzed using a UV–Vis spectrophotometer at 280 nm to determine the concentration of released Lfcin. Each experiment was taken in triplicate for three individual experiments.

2.7. Study of antibacterial activity of Lfcin-Nio

The bacterial suspension, previously adjusted to the 0.5 McFarland standard containing approximately 1 to 2 × 10^8 CFU/mL, was appropriately diluted to obtain a final concentration of 10^5 CFU/mL. The microtiter plate containing the different dilutions of niosomes was loaded with 100 µL of bacterial suspension to yield the final test concentration of bacteria, approximately 10^4 CFU/well, and incubated at 37 °C. The bacterial growth curve was generated by the continuous monitoring of turbidity at the optical density (O.D.) of 600 nm on a microplate reader. Drug control based on vancomycin (VAN) or meropenem (Mpm) at 8 µg/mL was also performed.

2.8. Mixed-culture biofilm formation in the channel µ-slide

The effects of Lfcin-Nio on biofilm formation were examined on a channel µ-slide. The mixed-culture biofilm was investigated as previously described, with some modifications (Pouget et al., 2022). Briefly, the drug-resistant bacteria (VISA-087 and PA-002R) were scraped from a plate and adjusted to a 0.5 McFarland standard. Polymicrobial cultures (1 × 10^5 CFU for each species) were seeded into the inflow well of a six-channel µ-Slide (ibidi USA Inc., WI, USA) and incubated at 37 °C for 48 h. The mature biofilm was then treated with Lfcin-Nio for another 24 h. The control wells contained Brain Heart Infusion (BHI) broth alone, empty-Nio, or 8× the minimum bactericidal concentration (MBC) of VAN-treated biofilm. After incubation, biofilms were live-dead stained with SYTO 9 Green Fluorescent Nucleic Acid Stain (Thermo Fisher Scientific Inc., MA, USA) and propidium iodide (PI) for 15 min in the dark, and were analyzed for biofilm formation with a confocal laser scanning microscope (CLSM) (Leica STELLARIS 5, Leica Biosystems, IL, USA). The LAS-X software (Leica Biosystems, IL, USA) was used for image acquisition and live/dead ratio analysis.

2.9. Preparation of Lfcin-Nio/hydrogel

The final concentration of 0.5 % *w/v* P188, 20 µg/mL EGF, and 10 % *v*/v Lfcin-Nio (or empty-Nio) was dissolved in cold, sterilized, distilled water. The addition of P407 was incorporated into the mixture to obtain the final concentration of 20 % w/v at 4 °C under stirring for 4 h and was stored at 4 °C until used.

2.10. Characterization of Lfcin-Nio/hydrogel

2.10.1. Gelation time

The gelation time of the hydrogels was measured using the vial inversion method (Tao et al., 2020). The blank hydrogel (hydrogel 1), empty-Nio/hydrogel (hydrogel 2), or Lfcin-Nio/hydrogel (hydrogel 3) were incubated at 37 °C. Gelation time is defined as the time required for no flow to be observed in each hydrogel formulation.

2.10.2. Rheological measurement

Rheological measurements of the hydrogels were examined using a rheometer (Modular Compact Rheometer MCR 302e, Anton Paar, Graz, Austria) with a parallel plate geometry. The hydrogel solutions were added and measured on the rheology plate at a temperature range of 20–40 °C and a heating rate of 1 °C/min. The variations of storage modulus (G') and the loss modulus (G") were measured under 0.1–100 % strain and a frequency of 0.01–100 Hz.

2.10.3. Swelling study

The lyophilized hydrogels (W_0) were weighed and immersed in PBS, pH 7.4 at 37 °C with shaking at 100 rpm. At designated time points, the

swollen hydrogels were obtained and excess liquid from the sample surface was removed and wiped off with tissue paper. The hydrogel samples were weighed (W_s) and the swelling ratio was calculated using the following equation:

Swelling ratio = $(W_s\text{-}W_0)/W_0 \times 100$ %.

2.10.4. Microscopic morphology of hydrogels

The surface and internal microscopic morphologies of the hydrogels were observed by scanning electron microscopy (SEM). In brief, hydrogels were frozen in liquid nitrogen, followed by freeze-drying. The lyophilized hydrogels were then sputter-coated with gold using a JEOL JFC-1100E Ion Sputtering device (JEOL, Tokyo, Japan) under vacuum and further subjected for SEM imaging.

2.11. In vitro antibacterial activity of Lfcin-Nio/hydrogel

Antibacterial-resistant strains, including VISA, *P. aeruginosa*, *E. coli*, and *K. pneumoniae,* were subjected to assess the antibacterial activity of Lfcin-Nio/hydrogels. The bacterial suspension (1×10^6 CFU/mL) was co-cultured with different hydrogel samples at an equal volume at 37 °C for 6 h. Following incubation, the bacterial viability was determined on Luria-Bertani (LB) agar plates and was counted as a colony-forming unit (CFU).

2.12. In vitro cytotoxicity of Lfcin-Nio/hydrogel

The cytotoxicity of the hydrogels was conducted based on the extraction solutions of the hydrogels by an indirect-extraction method as previously described (Cui et al., 2011) with some modifications. In brief, the hydrogel samples were immersed in a complete cell medium at a ratio of 1:1 and incubated at 37 °C, 5 % CO_2 for 1, 3, 5, and 7 days. Afterward, the samples were centrifuged at 1200 rpm at 4 °C for 5 min, and the supernatant of the extraction solutions was then collected. The cytotoxicity of the degrading products on cells was analyzed using a superKine™ Maximum Sensitivity Cell Counting Kit-8 (CCK-8) assay (Abbkine, GA, USA). Briefly, the cells (2×10^4 cells/well) were seeded in 96-well plates and cultured at 37 °C for 24 h. Each group of hydrogel extracts was added to the cells. After 24 h, 20 µL of CCK-8 solution was added to each well and incubated at 37 °C for another 1 h 30 min. The absorbance of the mixture was measured at 450 nm.

2.13. Cell settling experiment

Cell settling assay was performed according to Grosskopf et al., 2020 (Grosskopf et al., 2020), with some modifications. The cells (3×10^5 cells/mL) were stained with 2 µM calcein AM dye (Thermo Fisher Scientific Inc., MA, USA) for 30 min and were then loaded into the hydrogels. The cell-hydrogel mixture was injected into a cuvette and imaged on its side under a CLSM with an incubation chamber system at 37 °C (LSM 900; Zeiss, Oberkochen, Germany). The cuvette was then placed upright for 2 h and imaged on its side to assess cell settling.

2.14. Transcriptional regulation of inflammation-related genes using quantitative real-time PCR

The cells (1.5×10^5 cells) were pre-treated with medium containing 10 µg/mL of lipopolysaccharide (LPS) for 6 h, and further incubated with the hydrogel extracts for 24 h. To investigate the mRNA expression of *interleukin 1 beta* (*IL-1β*), *transforming growth factor beta* (*TGF-β*), and *cyclooxygenase-2* (*COX-2*), the total RNA of the treated cells was extracted using TRIzol reagent (Ambion, CA, USA) according to the manufacturer's instructions. A total of 500 ng of RNA was reversed transcribed into cDNA using Fasting gDNA dispelling RT SuperMix (TIANGEN Biotech (Beijing), BJ, China), and the amplifications were carried out using a SuperReal PreMix Plus (SYBR Green) (TIANGEN Biotech (Beijing), BJ, China). The sequences of primers used for *IL-1β, TGF-β, COX-2*, and *glyceraldehyde-3-phosphate dehydrogenase* (*GAPDH*), which was used as the internal control, are shown in Table 1. The PCR reactions included initial denaturation at 95 °C for 900 s, followed by 40 cycles of denaturation at 95 °C for 10 s, and annealing at 58 °C for 30 s. The relative fold change in the mRNA expression was analyzed using the $2^{-\Delta\Delta CT}$ method.

2.15. Cell scratch assay

The cells (1.5×10^5 cells) were seeded in 12-well plates for 24 h to achieve at least a 90 % confluency. The monolayer cell was scratched with a 200 µL pipette tip and washed with PBS to remove the floating cells. The initial scratch area of each treatment was measured as C_0. Then, the cells were treated with the extraction of the hydrogels and incubated at 37 °C in 5 % CO_2 for 24 h. The wound closure was imaged, and the wound width was recorded at 6, 12, and 24 h as C_t. The wound width ratio was computed using the following formula:

Wound width (%) = $(C_0\text{-}C_t)/C_0 \times 100$.

2.16. Statistical analysis

All results are represented as the standard error of the mean (SEM). Comparisons between groups were made using one-way analysis of variance (ANOVA) and Tukey's multiple comparisons test. Notably, $^*p < 0.05$ and $^{**}p < 0.01$ was considered statistically significant. The analyses and graphics were performed using GraphPad Prism version 9.0 (GraphPad Software Inc., CA, USA).

3. Results

3.1. Physicochemical characterization of Lfcin-Nio

The niosome formulations prepared from non-ionic surfactants and cholesterol with and without Lfcin, were fabricated and characterized. A schematic representation of Lfcin-Nio is shown in Fig. 1A. As shown in Fig. 1B, the particle size of the empty-Nio was 112.38 ± 23.28 nm with a negative charge of ZP, approximately −12.82 ± 0.04 mV. The particles significantly increased in size at 396.91 ± 20.96 nm upon loading Lfcin and produced a negative ZP of −10.5 ± 0.3 mV. The TEM images showed the spherical morphology of the particles and a homogeneous size distribution, as indicated by the PDI values ranging between 0.33 ± 0.04 and 0.38 ± 0.01 for empty-Nio and Lfcin-Nio, respectively (Fig. 1C and D). The EE of Lfcin-Nio was then determined using an indirect method at approximately 72.30 ± 7.05 % EE of Lfcin.

FT-IR spectroscopy was used to support the successful encapsulation of Lfcin in the niosome. In this study, the niosome formulations contained an optimal composition of non-ionic surfactants, including Tween 60, Span 80, and cholesterol, as reported in previous studies (Sangboonruang et al., 2021). The FT-IR spectrum of the niosome is shown in Fig. 1E. The O—H stretching vibration of the hydroxyl functional group of Tween 60, Span 80, cholesterol appeared in the region of 3362–3527 cm^{-1}. The C—H stretching of the aliphatic group of the surfactants and cholesterol appeared at 2197 and 2852 cm^{-1}. The C═O stretching vibration of the ester functional group in Tween 60 and Span

Table 1
The sequence of primers used in real-time PCR amplification.

Primers	Sequences (5′-3′)	Ref.
IL-1β	Fwd-CAG AAG TAC CTG AGC TCG CC Rev-AGA TTC GTA GCT GGA TGC CG	(Abuarqoub et al., 2022)
TGF-β	Fwd-GCC CTG GAC ACC AAC TAT TGC T Rev-AGG CTC CAA ATG TAG GGG CAG G	(Falanga et al., 2002)
COX-2	Fwd-ATC ATT CAC CAG GCA AAT TGC Rev-GGC TTC AGC ATA AAG CGT TTG	(Yang et al., 2022)
GAPDH	Fwd-GAA GGT GAA GGT CGG AGT C Rev-GAA GAT GGT GAT GGG ATT TC	(Janssens et al., 2004)

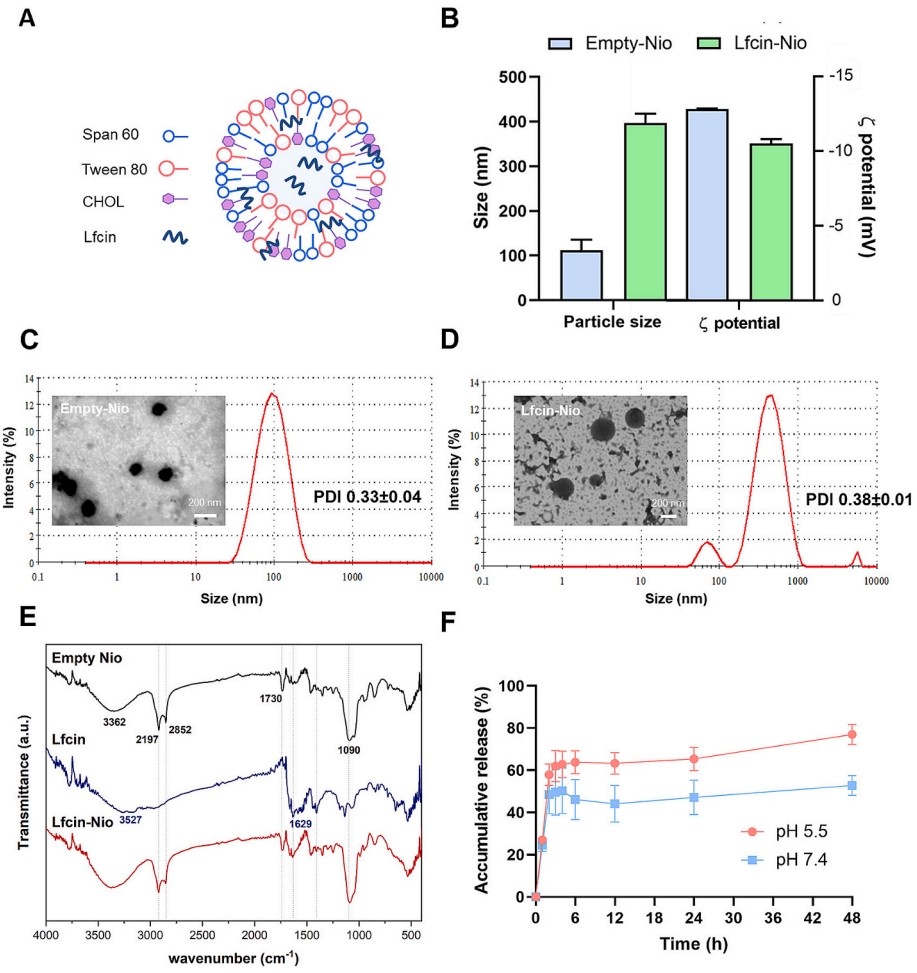

Fig. 1. The physicochemical characteristics of niosomes. (A) Schematic representation of Lfcin-Nio. (B) Average particle sizes and ZP of NPs. (C and D) Size distribution and morphology of empty-Nio and Lfcin-Nio, respectively. (E) FT-IR spectra of Lfcin-Nio. (F) Release profile of Lfcin-Nio at 37 °C, pH 5.5 and 7.4.

80 was observed at 1730 cm^{-1}. Moreover, the intense band at 1090 cm^{-1} was assigned to the C—O stretching vibration of the ester group of Tween 60 and Span 80. The FT-IR of Lfcin showed a peak at 1629 cm^{-1}, designated to the C═O stretching of the peptide (amide) bond (Luo et al., 2015; Almowalad et al., 2021), which was not present in the FT-IR spectra of empty-Nio and was used for the indication of the successful incorporation of Lfcin into the niosome.

Bacterial infections in wound tissues cause a mildly acidic microenvironment (Albright et al., 2017; Cheng et al., 2021), hence, the drug release profile of Lfcin was investigated. The results revealed that a lower pH (pH 5.5) has a significant influence on Lfcin release behavior, with more than 60 % of Lfcin released, compared with conditions at a pH of 7.4 where the released Lfcin was approximately 50 % (Fig. 1F). Moreover, a Lfcin-sustained release from niosomes occurred for up to 48 h. These results indicate the entrapment ability of the niosomes with the pH-responsive and sustained release behavior of Lfcin.

3.2. Antibacterial activity of Lfcin-Nio

The antibacterial activity of Lfcin-Nio was determined using optical density at 600 nm (OD_{600}) as shown in Fig. 2. Compared with the growth control, the empty-Nio had almost no effect on disinfecting bacteria. However, the growth inhibitory effect of the empty-Nio was observed in *S. aureus* ATCC25923 (SA), *P. aeruginosa* ATCC27853 (PA), and the clinical isolate of *P. aeruginosa* (PA-001). When treated with Lfcin-Nio, the antibacterial efficacy was found to be dose-dependent. Results show that Lfcin-Nio displayed bactericidal activity against SA, vancomycin-intermediate *S. aureus* (VISA-087), PA, and *E. coli* ATCC25922 (EC); while a bacteriostatic effect was found on *K. pneumoniae* ATCC700603 (KP), PA-001, and ESBL producing bacteria, including *K. pneumoniae* (KP-027R) and *E. coli* (EC-035R). In the drug-susceptible clinical isolates, the strains susceptible to Lfcin-Nio were found in the following order; PA-001 > *S. aureus* (SA-001) > *E. coli* (EC-001) > *K. pneumoniae* (KP-001). Whereas the drug-resistant groups showed more susceptibility to Lfcin-Nio in VISA-087 > *P. aeruginosa* (PA-002R) > KP-027R > EC-035R. Importantly, Lfcin-Nio (dilutions of 1:5 and 1:10) also showed a comparable result with 8 μg/mL of VAN and Mpm for drug-resistant *S. aureus* (VISA-087) and *P. aeruginosa* (PA-002R), respectively. For further experiments, the Lfcin-Nio-loaded hydrogel was prepared at a ratio of 1:10, Lfcin-Nio to hydrogel solution.

3.3. Anti-biofilm activity

To investigate the ability of Lfcin-Nio to eradicate bacterial cells residing in biofilms, the mature biofilms were analyzed in the channel μ slides. The biofilm samples were live-dead stained for analysis by a CLSM. Visualization of the biofilm structure in untreated and empty-Nio treated samples showed live cells (green) in the majority, while only a few dispersed dead bacteria (red) were observed (Fig. 3A and C). In contrast, 8 × MBC of VAN or Lfcin-Nio treated biofilms remarkably showed more dead cells distributed throughout the biofilm structure (Fig. 3B and D). Quantification of the live to dead ratio indicated approximately 84 % and 91 % of viable bacteria in the control and empty-Nio treated biofilms, respectively. Whereas the viable cells in the

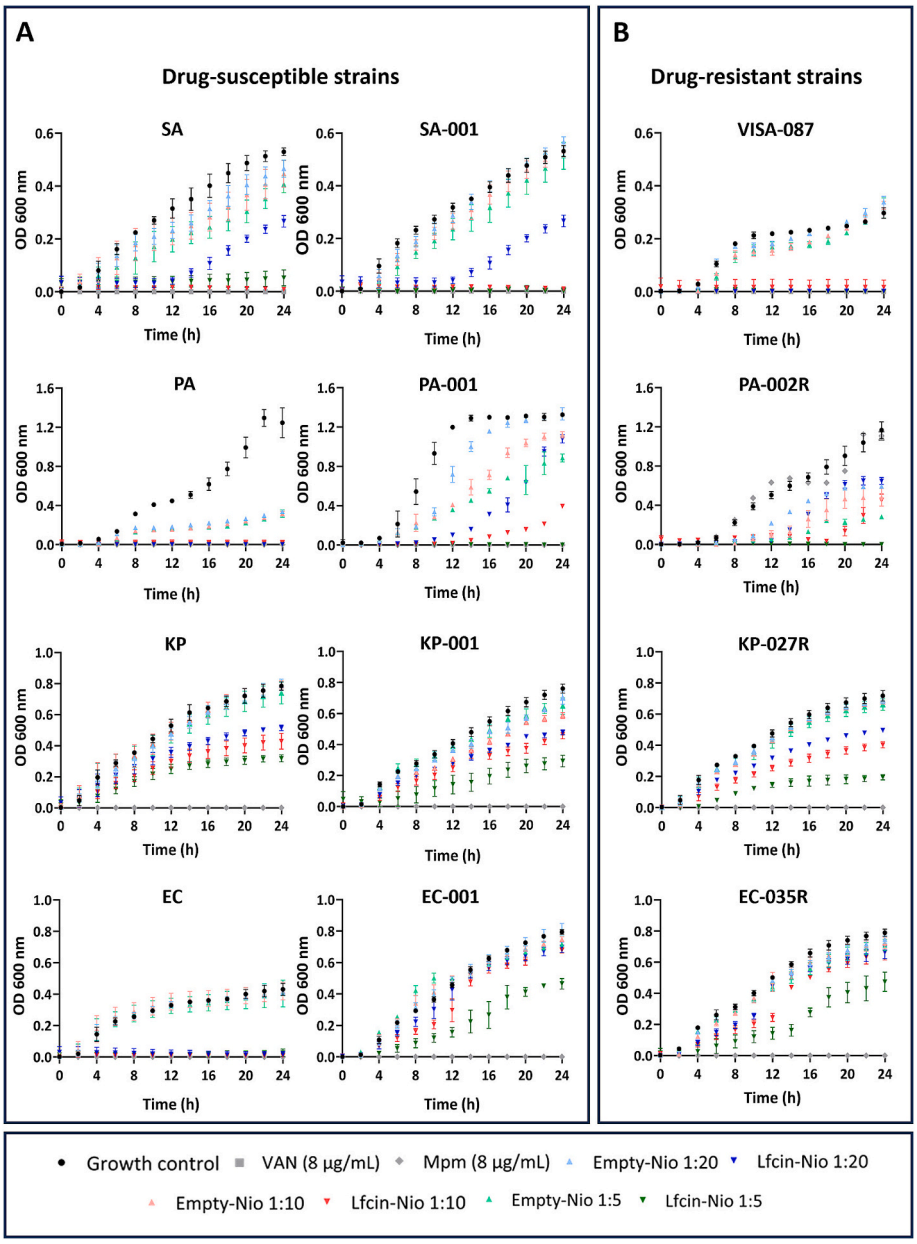

Fig. 2. Antibacterial activity of Lfcin-Nio against drug-susceptible and drug-resistant strains.

Lfcin-Nio treated biofilm were significantly reduced compared to empty-Nio (*$p < 0.05$), with 62 % live cell distribution. Noticeably, treating the dual-species biofilm with Lfcin-Nio prompted a killing activity similar to 8 × MBC of VAN treatment. These results indicate that biofilm treatment with Lfcin-Nio effectively induced bacterial cell death within the biofilm matrix.

3.4. *Physical and mechanical properties analysis of Lfcin-Nio/hydrogel*

To obtain the injectable hydrogel with thermo-responsive properties, P407 and P188 were introduced to the hydrogel network and were supplemented with EGF for the purpose of assisting tissue repair. This hydrogel construct without NPs was designated as a blank hydrogel (hydrogel 1). For the niosome-loaded hydrogel, the empty-Nio or Lfcin-Nio was homogeneously incorporated into the blank hydrogel to establish an empty-Nio-loaded hydrogel (hydrogel 2), and Lfcin-Nio-loaded hydrogel (hydrogel 3), respectively. The obtained hydrogel samples began as translucent and slightly viscous solutions (sol) at room temperature. The sol phase changed into a hydrogel (gel) after incubation at 37 °C, showing the sol-gel phase transition properties of the hydrogels and, hence, the formation of the cross-linking networks (Fig. 4A). Furthermore, the liquified solution could be continuously injected and was able to write the letters “CMU” through a syringe without resistance while maintaining a stable gel state (Fig. 4B). This proved the great injectability of the hydrogels. The gelation time of the hydrogels was evaluated by the vial inversion method performed for 30 s for hydrogels 1 and 2, and 15 s for hydrogel 3 (Fig. 4C), which was desirable gelation behavior and appropriate operation times for *in vivo* injection.

To gain further insight into the mechanical properties of the hydrogel structures, a rheological analysis was performed. All hydrogel samples were monitored by various amplitude sweeps from 0.01 to 100 % strain. The results showed that G’ and G" were constant among the 0.01–1 % strain, and that G" was lower than G’. When the amplitude sweeps were increased by more than 1 % strain, G’ was decreased and equivalent to the value of G" at a 5 % strain, indicating a deformation of the hydrogel

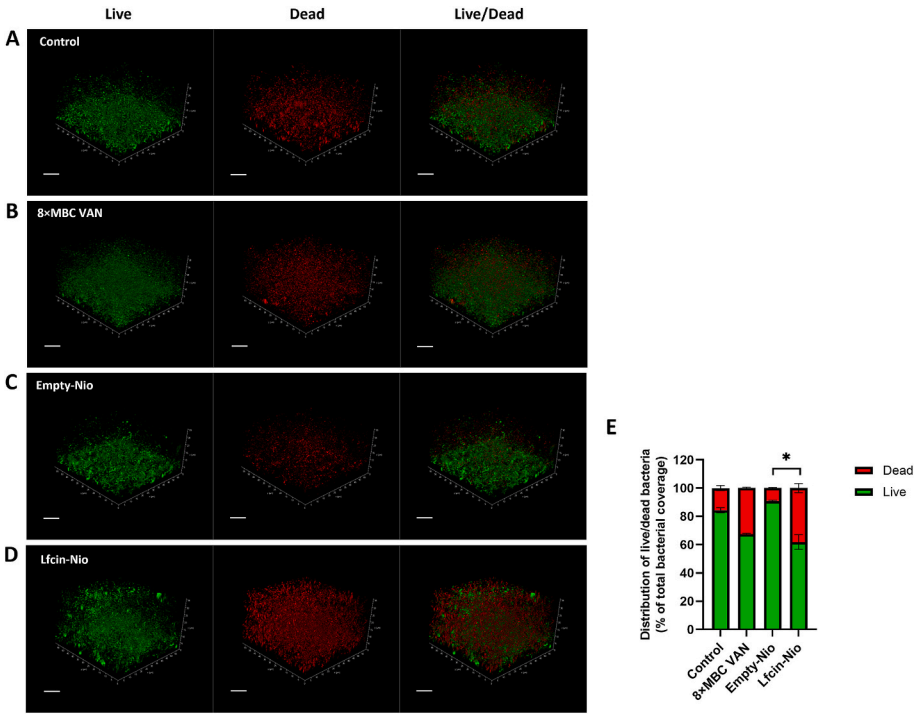

Fig. 3. Live-dead staining of dual-species biofilms after treatment with Lfcin-Nio. Pre-formed biofilms of VISA-087 and PA-002R were incubated for 24 h in (A) BHI broth (control), (B) 8 × MBC VAN, (C) empty-Nio, or (D) Lfcin-Nio, and were then stained with SYTO 9 and PI to show live (green) and dead (red) bacterial cells, respectively. The 3D images were acquired using CLSM with a magnification of 700×. Scale bars 10 mm. (E) The ratio of live/dead bacteria in dual-species biofilms was obtained from the mean fluorescent intensity of SYTO 9/PI and quantified by LAS-X software. $*p < 0.05$.

microstructures (Fig. 4D). From this result, the amplitude sweep at a 0.5 % strain was chosen to determine the dynamic rheological property within the linear viscoelastic region (LVR) of the hydrogel samples based on sweeping frequency (Fig. 4E). For all hydrogels, G' distinctly transcended G" with a sweep frequency varying from 0.1 to 100 rad/s. G' increased from 5600 Pa to over 10,500 Pa, while G" decreased from 2800 Pa to under 730 Pa. These results reflect the elastic and structural properties of the hydrogels.

The thermosensitive properties of the hydrogel samples were also examined at temperatures between 20 °C–40 °C. As shown in Fig. 4F and G at temperatures below 20 °C, the values of G', G", and G"/G' (viscosity) in all hydrogels exhibited low levels. The progressive increment in the magnitude of both moduli was observed, with G' being greater than G", when the temperature increased indicating the *in situ* formation of the hydrogels. Noticeably, hydrogel 3 had a higher viscosity than hydrogels 1 and 2 at the initial phase of measurement. This finding likely correlates to the short gelation time previously observed in hydrogel 3.

The swelling of hydrogels was investigated in PBS, pH 7.4 at 37 °C, mimicking the physiological conditions of the human body. The hydrogels with and without NPs showed rapid expansion during the first 6 h, then reached a state of equilibrium with approximately 3 folds of the swelling ratio (Fig. 4H). In addition, the porosity and surface structure of the hydrogels were also observed using a SEM. The cross-section SEM image showed an obvious porous structure with different microstructures and various interconnecting pores (Fig. 4I). The structure of the inner surface was further observed in hydrogels with and without NPs, as shown in Fig. 4J and K. The trapping of particles less than 500 nm by rough absorption surfaces was observed in NP-loaded hydrogels. This size was quite similar to the size of NPs previously observed by DLS and TEM. This finding confirms that the NPs were integrated with the hydrogel structure.

3.5. *In vitro antibacterial activity of Lfcin-Nio/hydrogel*

The antibacterial activity of Lfcin-Nio/hydrogels was investigated by determining the bacterial CFU. Drug-resistant strains of bacteria were chosen as models. The colony counting assay was performed after immersing the hydrogels into the bacteria solution for 6 h. As shown in Fig. 5, bacterial numbers treated with hydrogels 1 and 2 were not significantly different compared to the growth control. Hydrogel 3 exhibited significantly stronger antibacterial effects against VISA-087 and PA-002R ($**p < 0.01$), as colony forming was not found and slightly decreased the colony count of EC-035R. Nevertheless, KP-027R was not affected by all three hydrogels. These results suggest the potential activity of Lfcin-Nio/hydrogels for their bactericidal effects on drug-resistant *S. aureus* and *P. aeruginosa*.

3.6. *Cytotoxicity and cell settling of Lfcin-Nio/hydrogel*

The purpose of hydrogels is to be used as a biomaterial for clinical application in wound care, thus the primary requirement of hydrogels is safety. As shown in Fig. 6A, the fibroblast treated with extracts derived from each hydrogel sample exhibited high survival rates of more than 83 % after 24 h incubation, indicating the low cytotoxicity of the hydrogel samples. To assess whether hydrogels can maintain uniform cell suspensions and not induce cell settling, the calcein AM dye-labeled cells were loaded into the hydrogels, and gravity-driven cell settling was then examined. The results demonstrated the homogeneous distribution of cell behavior in the hydrogels and were not induced to precipitate after measurement for 2 h (Fig. 6B). These findings suggest that the hydrogels have biocompatibility, low toxicity, and mechanical properties to prevent cell settling.

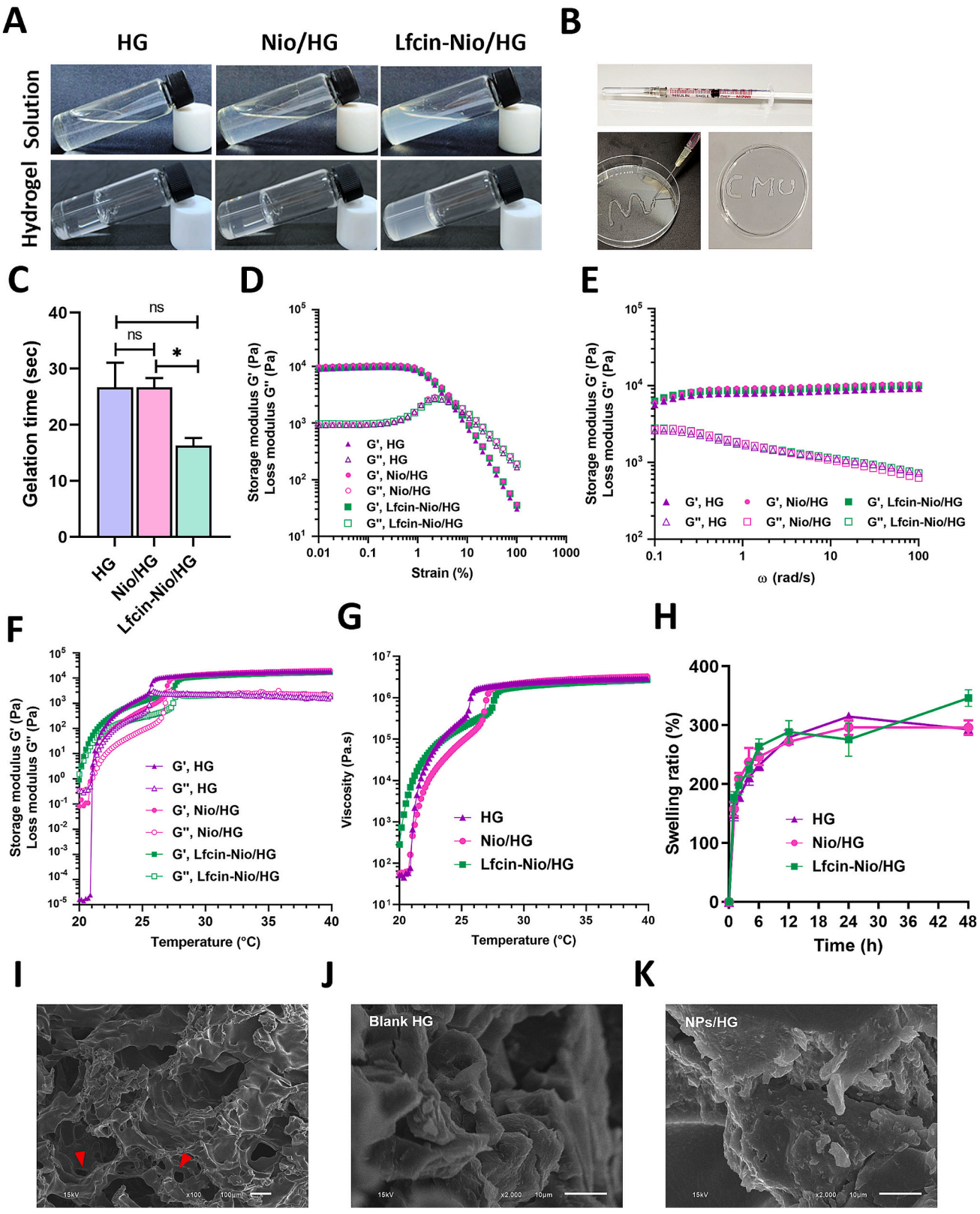

Fig. 4. Characterization of hydrogels. (A) Photographs of hydrogel samples in aqueous solutions in sol-gel states at 37 °C. (B) Photographs of the injectability of hydrogels. (C) Gelation time of the hydrogels with and without NPs. (D) Hydrogel amplitude scanning test. Measurements were carried out with a constant frequency (1 Hz). (E) Frequency sweep tests of the hydrogels. Sweep frequency varied from 0.1 to 100 rad/s with a constant of 0.5% for sweep frequency detections. Rheological properties exhibiting (F) storage modulus (G') and loss modulus (G"), and (G) viscosity of the hydrogel samples as a result of temperature. (H) Swelling rate of hydrogel samples after swelling for 48 h. Cross-sectional SEM images of (I) the porous structure of hydrogels on a scale of 100 mm and the interconnected pores (red arrowhead). (J and K) The enlarged SEM images of (J) blank hydrogels and (K) NP-loaded hydrogels, scale bar of 10 mm. HG: blank hydrogel; Nio/HG: empty-Nio/hydrogel; Lfcin-Nio/HG: Lfcin-Nio/hydrogel.

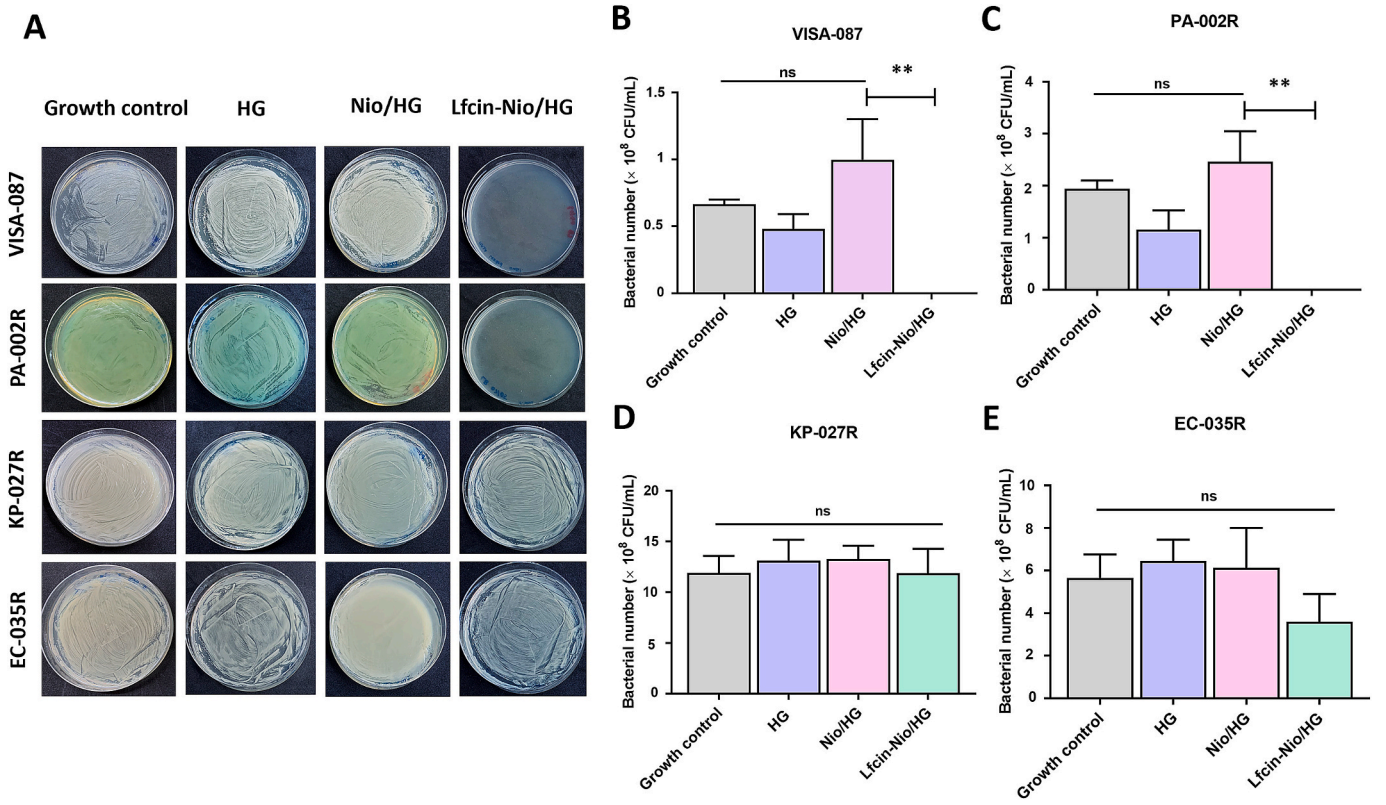

Fig. 5. Antibacterial activity of hydrogels against drug-resistant bacteria. (A) Colony counting assay, and the quantity of bacterial cell numbers (B) VISA-087R, (C) PA-002R, (D) KP-027R, and (E) EC-035R. $^{**}p < 0.01$, ns represents no significance. HG: blank hydrogel; Nio/HG: empty-Nio/hydrogel; Lfcin-Nio/HG: Lfcin-Nio/hydrogel.

3.7. Cell scratch healing and anti-inflammatory properties of Lfcin-Nio loaded hydrogel

The cell scratch assay was employed to determine the effects of hydrogels on cell migration and scratch healing ability. The cell scratch was imaged at 0, 6, 12, and 24 h to calculate the rate of wound closure. The results show that the cells treated with hydrogels had a tendency to grow and migrate faster than the untreated cells (Fig. 6C and D). Interestingly, there were significant differences in hydrogel 3 compared to cell control and hydrogel 2 in the first 6 h ($^{*}p < 0.05$). The results demonstrated that the wound width was reduced by 54.80 % in cells treated with hydrogel 3, while the wound width of the control group remained at more than 60 %. At 12 h, the hydrogel 3-treated cells showed a significantly smaller wound area by 5.80 % ($^{**}p < 0.01$ when compared to cell control and hydrogel 1 and $^{*}p < 0.05$ when compared to hydrogel 2). On the other hand, the cell control, hydrogel 1, and hydrogel 2-treated cells maintained a wound width of 44–58 %. These results conclude that hydrogel 3 had a greater ability to accelerate the healing of wound scratches.

Inflammatory reactions are responsible for infections and tissue injuries, and long-term inflammation contributes to delayed or non-healing wounds. Thus, the anti-inflammatory function of hydrogels can support their therapeutic effects. In this study, the key pro-inflammatory cytokines and inflammatory mediators such as *IL-1β, TGF-β*, and *COX-2* were assessed in the cells that were pre-activated with LPS. As shown in Fig. 6E-G, all hydrogel samples showed significantly reduced mRNA expression levels of *IL-1β* ($^{*}p < 0.05$) and *COX-2* ($^{**}p < 0.01$), whereas the expression of *TGF-β* was not changed. It was noticed that the fold changes of gene expression showed no remarkable difference in each hydrogel sample. These results suggest that the hydrogels possibly exhibit anti-inflammatory properties through the suppression of *IL-1β* and *COX-2,* which were assigned as important therapeutic targets in clinical treatment.

4. Discussion

Chronic wounds are caused by the delayed recovery of injured tissue, often resulting from insufficient treatment of acute traumatic wounds, and even some chronic diseases such as diabetes and cancers. Impaired wound healing is often caused by the reduction of tissue growth factors, an increase in proteolytic enzymes such as matrix metalloproteinase, an increase of inflammatory mediators, and the presence of senescent cells (Monika et al., 2021).

Moreover, the most common complication in delayed chronic wound healing is associated with bacterial infection, which can create prolonged inflammation and lead to the destruction of the extracellular matrix and fibroblast production. In worst-case scenarios, deep infection *via* the spreading of causative agents may progress to systemic infection, and eventually, surgical amputation (Powers et al., 2016; Monika et al., 2021). The World Health Organization (WHO) has concerned with antimicrobial resistance and around 50 % of infections associated with *E. coli*, *K. pneumoniae*, *S. aureus*, and *P. aeruginosa* show resistance against the most effective antimicrobials (Puca et al., 2021; World Health Organization, 2024). Reducing the consumption of antibiotics based on alternative therapeutic agents, such as AMPs, has been considered as an emerging class of drugs for the treatment of traumatic infections (Ding et al., 2022).

For several years, the natural bioactive Lfcin has been recognized as a wide-spectrum antimicrobial agent (Ohradanova-Repic et al., 2023), and its safety has been stated in previous reports (Intorasoot et al., 2022; Ohradanova-Repic et al., 2023). In this study, innovative clinical treatments based on nanotechnology were employed to improve the therapeutic efficacy of Lfcin through a niosomal drug delivery system. Corresponding with our previous work, we successfully encapsulated

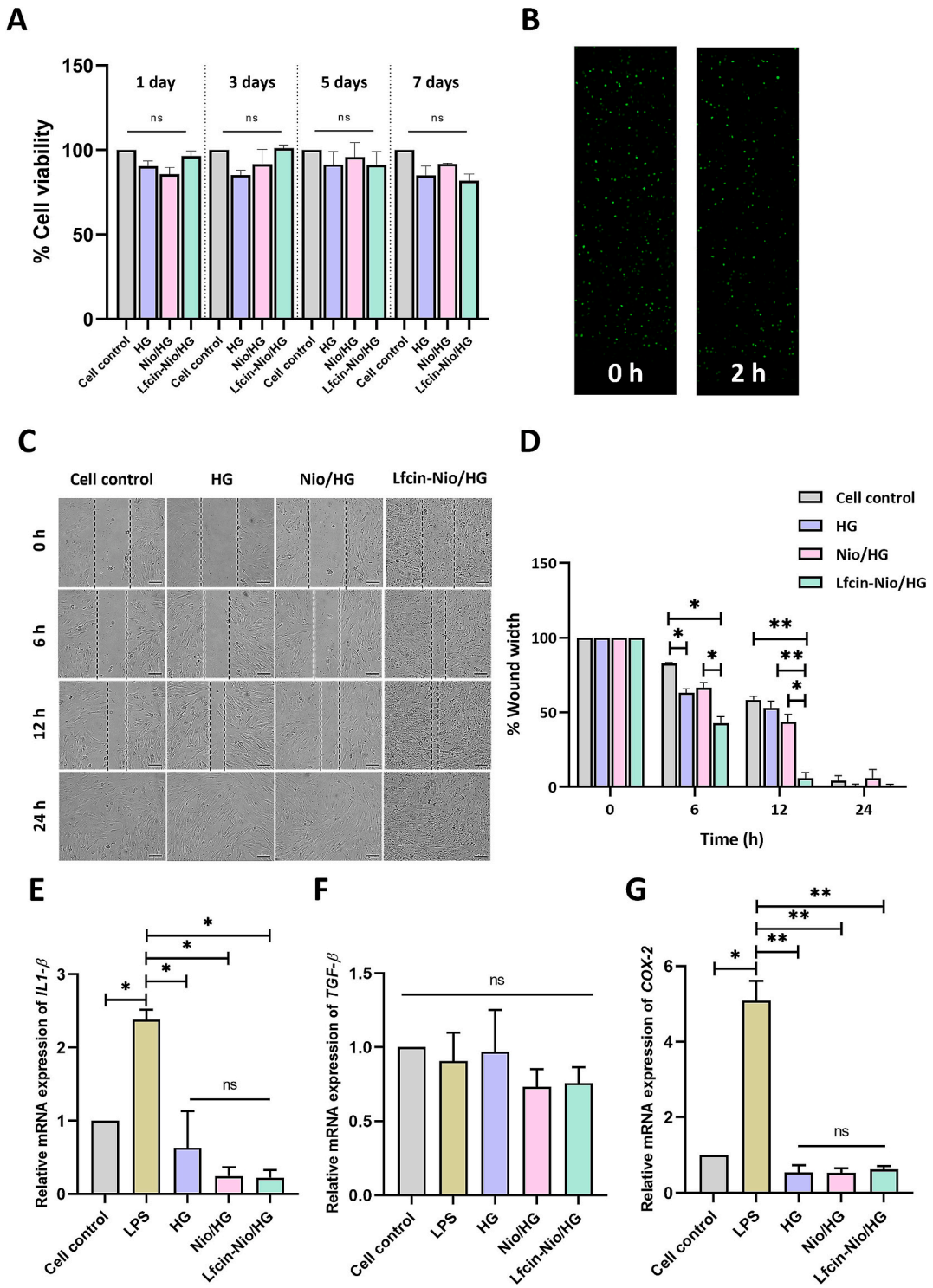

Fig. 6. Biological properties of hydrogels. (A) *In vitro* cytotoxicity assessment of hydrogels on CCD1123-sk cells. The hydrogel samples were immersed in a complete cell medium at a ratio of 1:1 and incubated at 37 °C, 5%CO_2 for 1, 3, 5, and 7 days. The cells were treated with hydrogel extracts for 24 h, and cell viability was evaluated by CCK-8 assay. (B) Cell settling behaviors in hydrogels across 2 h. The cells were pre-stained with calcein AM dye, and then loaded into the hydrogels. Cell distribution in the hydrogels was observed under a CLSM with a magnification of 10×. (C and D) Cell wound scratch assay of CCD1123-sk cells. The cells were scratched and then treated with hydrogel extracts. The wound areas were recorded at different time points and the quantitative scratch area was analyzed. (E-G) Effects of hydrogels on the expression of inflammation-related genes such as *IL-1b, TGF-b,* and *COX-2*. The mRNA levels of treated cells were assessed by quantitative real-time PCR. Relative mRNA expression was normalized to GAPDH as the internal control, and expression levels are represented as a fold change of 2^{-DDCT} compared to the control. All scale bars are 50 mm. *$p < 0.05$, **$p < 0.01$. HG: blank hydrogel; Nio/HG: empty-Nio/hydrogel; Lfcin-Nio/HG: Lfcin-Nio/hydrogel.

melittin, one class of cationic AMP (Sangboonruang et al., 2021). The optimized formulation was further applied for Lfcin, and significant parameters were characterized. The particle sizes of Lfcin-Nio presented in the nanoscale with PDI values (0.33–0.38) indicate uniformity in the formulation (Fig. 1B-D). The particle size of Lfcin-Nio reached approximately 400 nm, which was larger than that of the empty particles (100 nm) due to the containment of the payload peptide. Moreover, the effects of repulsive force between the particles presented by the ZP values were also generally considered. Results show that Lfcin-Nio had a negative charge with a ZP of −10 mV, which might not be an effective electric charge that easily contributes to the aggregation of NPs (Sangboonruang et al., 2021). Regarding the particles carrying a weak ZP, long-term stability needs to be considered and further investigation is required. The EE of Lfcin-Nio was approximately 70 %, which is found lower than our previous study which demonstrated more than 90 % EE of niosome loaded with melittin. These results could support the explanation that the number of positively charged residues (Arginine + Lysine) of AMPs possibly affects an interaction between the AMP and anionic niosomes, as well as the efficiency of the formulation to entrap the peptide (Sangboonruang et al., 2021). Furthermore, the presence of Lfcin in the Nio formula was also indicated by the functional groups corresponding to the FT-IR spectra (Fig. 1E). Moreover, the release profile of Lfcin-Nio was evaluated in a relevant, mildly acidic microenvironment resulting from bacterial infection, including infected wound tissue (Zhang et al., 2022). From the results, Lfcin-Nio exhibited a sustained release behavior, and the release rate in acidic conditions was greater than the rate in a physiological state (Fig. 1F).

Generally, most chronic wound infections are colonized by polymicrobial isolates. Gram-positive bacteria, particularly *S. aureus,* usually occupy the first week of the initial phase, followed by Gram-negative bacteria such as *P. aeruginosa*, *A. baumannii*, and *Enterobacteriaceae* (Ding et al., 2022). Notably, the rate of infection associated with antibiotic-resistant microorganisms has been increasing. Since a high prevalence of drug-resistant pathogens was found for *S. aureus*, *E. coli*, *K. pneumoniae*, and *P. aeruginosa* (Puca et al., 2021), drug-susceptible and drug-resistant strains of these species were employed in this study. Fig. 2 shows that the growth kinetics of bacteria gradually decreased in a dose-dependent manner after exposure to Lfcin-Nio, compared to the empty-Nio groups and growth control. Importantly, it clearly demonstrated the bactericidal activity of Lfcin-Nio against drug-susceptible and drug-resistant strains of *S. aureus* and *P. aeruginosa* as well as *E. coli* ATCC25922. These obtained results indicate the antibacterial activity of Lfcin-Nio through membrane permeability triggered by the released Lfcin (Ohradanova-Repic et al., 2023). Interestingly, among the drug-resistant strains, Lfcin-Nio showed the highest efficacy against VISA, likely due to the anionic-rich membrane of VISA (Sangboonruang et al., 2021). However, a bacteriostatic effect was observed in *K. pneumoniae* and *E. coli*, particularly in both drug-sensitive and drug-resistant clinical isolates. These results support previous studies by Morici et al., 2017 (Morici et al., 2017). Since it is known that natural resistance to Lfcin is found in some bacterial species (Ulvatne et al., 2002), one mechanism to explain low susceptibility to Lfcin is the induction of a transient loss of membrane potential (Morici et al., 2023). It has been demonstrated that the bacterial capsule can disrupt the electrostatic and hydrophobic interactions that protect the bacterial membrane from AMPs (Morici et al., 2023). Another possible reason involves the outer membrane protein T (OmpT) in *E. coli*, which acts as a protease responsible for resistance to AMPs (Ulvatne et al., 2002).

We further investigated Lfcin-Nio activity on biofilm, an extracellular polymeric substance (EPS) produced by microorganisms. The EPS is composed of polysaccharides, lipids, proteins, and nucleic acids, and achieves adhesion and cohesion in biofilm structures on solid surfaces through electrostatic forces, van der Waals forces, and hydrogen bonding. Moreover, biofilm acts as a protective barrier against mechanical and chemical stresses (Ahsan et al., 2024). Therefore, it has developed a crucial characteristic structure in wounds that promotes chronicity and inflammatory responses, as well as increases antimicrobial tolerance (Pouget et al., 2022). Previous evidence suggested that *S. aureus* and *P. aeruginosa* were the most common bacteria isolated from chronic wounds, and that co-infection showed more virulence (Serra et al., 2015) and increased biofilm formation (Pouget et al., 2022). In this study, the mixed-culture biofilm of drug-resistant *S. aureus* (VISA) and *P. aeruginosa* (PA-002R) was examined. Lfcin-Nio treated mature biofilm demonstrated notable dead bacteria distribution in the biofilm. Moreover, treating biofilm with Lfcin-Nio also increased bacterial death at a similar level in treatment with 8 × MBC VAN (Fig. 3E). These results reveal the significant antimicrobial effects of Lfcin-Nio on eradicating the cluster of bacteria embedded in the biofilm, which might occur through biofilm penetration and the fusion of niosomes with bacterial cell membrane (Haddadian et al., 2022; Barani et al., 2023). The main factor affecting the abilities of the lipid-based nanocarrier (LNC) against the complex nature of EPS is based on a diffusion coefficient, which is influenced by the NP constituents, particle size, and biofilm composition (Ahsan et al., 2024). Moreover, the negative or neutral LNC provides greater penetration. Whereas the cationic NP usually exhibits strong electrostatic interactions with the negative biofilm, which retains the NPs on the biofilm surface and limits their penetration (Alhariri et al., 2017; Ahsan et al., 2024).

In chronic wound care, a standard regimen for treating wounds is based on the use of dressings in combination with various secondary treatments. However, conventional wound dressings remain limited and insufficient for persistent wounds with infections (Zhang et al., 2020). To effectively manage bacterial wound infections, a functional wound dressing was constructed to eliminate bacterial burden and promote wound repair. In recent years, the use of various types of hydrogels composed of functional agents has gained a lot of attention (Pourjavadi et al., 2021). In the biomedical field, poloxamers are commonly used to form a reverse thermo-responsive, *in situ* hydrogel for prolonged drug delivery and a controlled release vehicle for biomolecules such as interleukin-2 (IL-2), bone morphogenic protein (BMP), urease, insulin, as well as EGF (Zhang et al., 2015). Herein, an injectable thermo-responsive poloxamer hydrogel was prepared based on P407 combined with P188, and supplemented with EGF. Furthermore, the Lfcin-Nio (or empty-Nio) was incorporated with the hydrogel. The hydrogel samples showed liquid-like materials at room temperature, while underwent the sol-gel phase transition at 37 °C with a reasonably short gelation time (within 20–30 s) (Fig. 4A and C). Noticeably, the gelation time of Lfcin-Nio-loaded hydrogels significantly decreased compared with the control hydrogels. This might be due to the more rigid network caused by the strong interaction of the NPs and the polymer network that increases the gel viscosity (Giuliano et al., 2018). Moreover, the hydrogels demonstrated a good injectability (Fig. 4B), suggesting the familiarity of the hydrogels with the anatomical structure of the skin. As the fluid-like and free-form injectable material, it is able to fill in deep wounds and then turn into a solid gel triggered by the skin wound temperature to protect the wounds and promote tissue regeneration (Zhou et al., 2022).

To further understand the behavior of hydrogels and their mechanical properties, the rheological characteristics were then elucidated. Hydrogels possess both viscous and elastic behaviors, also known as viscoelastic, commonly represented by G', G", and the ratio of G"/G' (Hu et al., 2020). From the rheological analysis as shown in Fig. 4D and E, all samples show the formation of hydrogels, representing G' exceeded by G". The deformation of the hydrogels occurred when the applied strain reached more than 1 %, exceeding the LVR, which resulted in the collapse of networks. For thermo-responsive hydrogels, the effect of temperature on the properties of the hydrogel samples was then investigated (Fig. 4F and G). At temperatures below 20 °C, the hydrogels exhibited low flowability values in G', G", and viscosity. The G', G", and the viscosity values rapidly increased when the temperature was increased, turning to the formation of the gel state with the greatest viscosity at 27–40 °C. This result implies that the hydrogels

demonstrated the gelation behavior in response to different temperature ranges of human skin. The gelation mechanism of thermo-responsive hydrogel is based on the interaction between the molecular structure of poloxamers and water molecules. When the temperature increases, a hydrogen bond between the solvent and the hydrophilic chain of the copolymer will fracture. These result in the rearrangement of poloxamer micelles to a cubic structure and then form a hexagonal structure that promotes the gelation process (Russo and Villa, 2019; Chen et al., 2021). Interestingly, among all samples, the hydrogels containing Lfcin-Nio had the greatest G' and G" values in the initial phase of measurement, suggesting a simpler and faster gel formation that is in concordance to previous results showing a short gelation time. This is possibly due to the crosslinking density of the hydrogel matrix, as well as the NPs immobilized covalently and non-covalently within gel networks (Giuliano et al., 2018; Syed Azhar et al., 2022). Additionally, being composed of peptides could increase intermolecular hydrogen bonding, which affects the gelation properties and the mechanical strength of hydrogels (Binaymotlagh et al., 2022). Hydrogel swelling behavior is also a critical property to determine its ability to absorb water through the association of three-dimensional macromolecule chains (Feng and Wang, 2023). From the results, all hydrogel samples possessed a high swelling ratio (Fig. 4H) indicating viscoelastic properties (Khan et al., 2023). Considering the microstructure of the hydrogels, as shown in the SEM results (Fig. 4I-K), it is suggested that the high-water absorbability of hydrogels is possibly due to their abundantly porous structure. From these results, it could be denoted that the porous network existing in the constructed hydrogels will not allow only water uptake and assimilate excess exudate from the wound, but will also facilitate sustained drug release, the entry of cells, and the exchange of nutrients (Tao et al., 2020; Jacob et al., 2021).

Besides its potential mechanical properties, the highest purpose of Lfcin-Nio/hydrogels is bacterial eradication and the promotion of wound healing. The antibacterial activity of hydrogels was investigated using antibiotic-resistant bacteria strains, and the hydrogels with Lfcin-Nio exhibited proficient antibacterial effects only on VISA and *P. aeruginosa,* leaving no surviving bacteria (Fig. 5). These findings are in accordance with the previous study on bacteria treated with Lfcin-Nio (Fig. 2). Determination of toxicity was also conducted on hydrogels to ensure their safety. The human skin fibroblast cells, after being co-incubated with degrading materials in hydrogel extracts, showed a survival rate of more than 83 % (Fig. 6A), and the cell behavior in the hydrogels proceeded as homogeneous dispersion with no precipitation (Fig. 6B). These observations confirmed the *in vitro*, non-cytotoxicity, and biocompatibility of hydrogels, which might be beneficial for further application *in vivo*.

Functional Lfcin-Nio/hydrogels were assessed to promote the wound healing process based on cell scratch assay. It is well known that EGF has been recognized as an excellent wound healing agent and is widely employed in conjugation with various platforms, such as ointments, liquid formulations, polymer patches, nanofiber, and hydrogels (Kim et al., 2016). The binding of EGF and EGF receptors (EGFR) on cell surfaces activates the signaling proteins *via* the RAS-RAF-MEK-MAPK pathway, which regulates cell cycle progression, cell proliferation, wound healing, and tissue homeostasis (Riesco et al., 2017). In the current study, the hydrogel-based formulations were supplemented with EGF to promote the healing process. Surprisingly, the obtained results revealed that the cells treated with Lfcin-Nio/hydrogels had a significantly more rapid rate of wound closure of almost 50 % within 6 h, while the control hydrogels showed insignificant wound closure rates compared to the untreated cells. Furthermore, the wound scratch areas showed nearly complete healing of approximately 95 % wound closure at 12 h after hydrogel 3 treatment (Fig. 6D). In this study, the effects of Lfcin on inducing rapid healing were found in concordance with the previous report (Mouritzen et al., 2021). Moreover, the supportive wound healing function can be found in poloxamers promoting cell proliferation and EGF production (Feng et al., 2021).

Inflammatory reactions are responsible for triggering infections and tissue injuries, and also serve as critical regulations during the wound healing process, through the activation of several pro-inflammatory cytokines and inflammatory mediator production (Ding et al., 2022; Schilrreff and Alexiev, 2022). For better understanding, we investigated the effects of the hydrogel-treated cells related to the inflammatory response. Currently, the key inflammatory mediators produced by fibroblasts are under investigation. This study revealed that all hydrogel-treated cells had great potency to down-regulate the mRNA expression of *IL-1β* and *COX-2*, while the mRNA level of *TGF-β* showed no significant alteration (Fig. 6E-G). Since there was no difference in the fold change of mRNA levels in either blank hydrogel treatment or hydrogels with or without NPs treatment, it was noted that the reduction of *IL1-β* and *COX-2* was possibly due to the effects of EGF or poloxamers present in all hydrogel samples. As mentioned, EGF is known to promote skin growth and homeostasis. The role of EGF involving the reduction of *IL-1β* in this study is correlated to the previous study demonstrating the decreased level of inflammatory cytokines, including IL-1, after the treatment of EGF and hyaluronate (HA)-EGF conjugates (Kim et al., 2016). In agreement with the earlier statement, a reduction of IL-1β could be a result of the progression of wound healing (Feng et al., 2021; Eggers et al., 2022). Aside from EGF, the previous study also revealed the effects of poloxamers on inhibiting IL-1β at mRNA and protein expression levels (Feng et al., 2021). IL-1β is a critical proinflammatory cytokine that participates in pathogen clearance and the inflammation phase of wound healing through activating downstream cascades (Xiao et al., 2020; Eislmayr et al., 2022). However, the accumulation of prolong inflammation, especially chronic wound infection, can impair the healing process. Therefore, IL-1β has been considered as a potential therapeutic target for treating delayed tissue repair (Dai et al., 2021). Likewise, it was reported that P188 also reduces inflammation, and the administration of P188 contributes to the suppression of COX-2 (Hunter et al., 2010). COX-2 is a pivotal mediator of inflammatory pathways, and the development of the COX-2 inhibitor is introduced as a promising inflammation treatment (Ju et al., 2022). Hence, hydrogels inhibiting COX-2 could enhance the therapeutic outcome of inflammatory reactions.

However, the alteration of the *TGF-β* mRNA expression did not depend on hydrogel treatment. This might suggest that rapid wound closure was regulated by other molecules, including EGF, Lfcin, and poloxamers, as stated elsewhere. In fact, TGF-β has been shown to play an essential role in the suppression of inflammation, the formation of ECM, and the proliferation of fibroblast and epithelial cells (Wong and Guillaud, 2004; Yoshimura et al., 2010). Furthermore, TGF-β is composed of three isomers (TGF-β1, TGF-β2, and TGF-β3) which present their expression levels and functions in different stages during skin repair (Feng et al., 2021). These results suggest that the polymer-based hydrogels containing EGF could be a potential mechanism for suppressing the *IL-1β* and *COX-2* expressions, which would be a potential therapeutic target to antagonize the inflammatory reaction.

In conclusion, the Lfcin-Nio/hydrogels not only exhibited antibacterial effects, but also exerted efficiency in accelerating wound closure. Moreover, the hydrogels had excellent anti-inflammatory properties through the down-regulation of the *IL-1β* and *COX-2* expressions. Taken together, the Lfcin-Nio/hydrogels appear to be a promising and advanced wound dressing achieving pathogen eradication, especially on drug-resistant *S. aureus* and *P. aeruginosa*, promoting wound repair, and preventing prolonged chronic inflammation. However, additional *in vivo* evaluation is necessary to gain insight into its potential benefits for future applications.

Funding

This research was funded by the Murata Science Foundation (MSF) and partially supported by Chiang Mai University (CMU Proactive Researcher, Chiang Mai University).

CRediT authorship contribution statement

Sirikwan Sangboonruang: Writing – review & editing, Writing – original draft, Project administration, Methodology, Investigation, Funding acquisition, Formal analysis, Data curation, Conceptualization. **Natthawat Semakul:** Writing – review & editing, Writing – original draft, Resources, Investigation, Formal analysis, Data curation. **Kiattikhun Manokruang:** Writing – review & editing, Resources, Methodology, Investigation, Formal analysis, Data curation. **Nuttawut Khammata:** Investigation, Formal analysis. **Kanyaluck Jantakee:** Investigation, Formal analysis. **Katanchalee Mai-Ngam:** Writing – review & editing, Resources. **Satrawut Charoenla:** Writing – review & editing, Resources. **Phadungkiat Khamnoi:** Resources. **Kanokwan Saengsawang:** Resources. **Usanee Wattananandkul:** Writing – review & editing, Resources. **Sorasak Intorasoot:** Writing – review & editing, Resources, Data curation. **Khajornsak Tragoolpua:** Writing – review & editing, Supervision, Resources, Methodology, Funding acquisition, Formal analysis, Data curation, Conceptualization.

Declaration of competing interest

The authors declare that they have no known competing financial interests or personal relationships that could have appeared to influence the work reported in this paper.

Data availability

Data will be made available on request.

Acknowledgements

We thank Ms. Supattra Suwanpairoj, application specialist, Rushmore Precision Co., Ltd., Bangkok, Thailand, for supporting the confocal laser scanning microscope. We thank Assoc. Prof. Dr. Ratchada Cressey, Department of Medical Technology, Faculty of Associated Medical Sciences, Chiang Mai University for supporting the instruments. We also thank Julia Marie Akins for the professional proofreading and editing of the manuscript.

References

Abuarqoub, D., Aslam, N., Zaza, R., Jafar, H., Zalloum, S., Atoom, R., Alshaer, W., Al-Mrahleh, M., Awidi, A., 2022. The immunomodulatory and regenerative effect of biodentine on human THP-1 cells and dental pulp stem cells: in vitro study. Biomed. Res. Int. 2022, 2656784. https://doi.org/10.1155/2022/2656784.

Ahsan, A., Thomas, N., Barnes, T.J., Subramaniam, S., Loh, T.C., Joyce, P., Prestidge, C. A., 2024. Lipid nanocarriers-enabled delivery of antibiotics and antimicrobial adjuvants to overcome bacterial biofilms. Pharmaceutics 16 (3), 396. https://doi.org/10.3390/pharmaceutics16030396.

Albright, V., Zhuk, I., Wang, Y., Selin, V., van de Belt-Gritter, B., Busscher, H.J., van der Mei, H.C., Sukhishvili, S.A., 2017. Self-defensive antibiotic-loaded layer-by-layer coatings: imaging of localized bacterial acidification and pH-triggering of antibiotic release. Acta Biomater. 1 (61), 66–74. https://doi.org/10.1016/j.actbio.2017.08.012.

Alhariri, M., Majrashi, M.A., Bahkali, A.H., Almajed, F.S., Azghani, A.O., Khiyami, M.A., Alyamani, E.J., Aljohani, S.M., Halwani, M.A., 2017. Efficacy of neutral and negatively charged liposome-loaded gentamicin on planktonic bacteria and biofilm communities. Int. J. Nanomedicine 18 (12), 6949–6961. https://doi.org/10.2147/IJN.S141709.

Almowalad, J., Somani, S., Laskar, P., Meewan, J., Tate, R.J., Mullin, M., Dufes, C., 2021. Lactoferrin-bearing gold nanocages for gene delivery in prostate cancer cells in vitro. Int. J. Nanomedicine 30 (16), 4391–4407. https://doi.org/10.2147/IJN.S316830.

Barani, M., Paknia, F., Roostaee, M., Kavyani, B., Kalantar-Neyestanaki, D., Ajalli, N., Amirbeigi, A., 2023. Niosome as an effective nanoscale solution for the treatment of microbial infections. Biomed. Res. Int. 16 (2023), 9933283. https://doi.org/10.1155/2023/9933283.

Binaymotlagh, R., Chronopoulou, L., Haghighi, F.H., Fratoddi, I., Palocci, C., 2022. Peptide-based hydrogels: new materials for biosensing and biomedical applications. Materials (Basel). 15 (17), 5871. https://doi.org/10.3390/ma15175871.

Chen, Y., Lee, J.H., Meng, M., Cui, N., Dai, C.Y., Jia, Q., Lee, E.S., Jiang, H.B., 2021. An overview on thermosensitive oral gel based on poloxamer 407. Materials (Basel). 14 (16), 4522. https://doi.org/10.3390/ma14164522.

Cheng, H., Long, L., Cao, J., Zhang, S., Wang, Y., 2021. Dual-crosslinked mussel-inspired smart hydrogels with enhanced antibacterial and angiogenic properties for chronic infected diabetic wound treatment via pH-responsive quick cargo release. Chem. Eng. J. 411, 128564. https://doi.org/10.1016/j.cej.2021.128564.

Cui, Z., Lee, B.H., Pauken, C., Vernon, B.L., 2011. Degradation, cytotoxicity, and biocompatibility of NIPAAm-based thermosensitive, injectable, and bioresorbable polymer hydrogels. J. Biomed. Mater. Res. A 98 (2), 159–166. https://doi.org/10.1002/jbm.a.33093.

Dai, J., Shen, J., Chai, Y., Chen, H., 2021. IL-1b impaired diabetic wound healing by regulating MMP-2 and MMP-9 through the p38 pathway. Mediators Inflamm. 2021, 6645766. https://doi.org/10.1155/2021/6645766.

Ding, X., Tang, Q., Xu, Z., Xu, Y., Zhang, H., Zheng, D., Wang, S., Tan, Q., Maitz, J., Maitz, P.K., Yin, S., Wang, Y., Chen, J., 2022. Challenges and innovations in treating chronic and acute wound infections: from basic science to clinical practice. Burns. Trauma. 10, tkac014. https://doi.org/10.1093/burnst/tkac014.

Eggers, B., Stope, M.B., Marciniak, J., Mustea, A., Deschner, J., Nokhbehsaim, M., Kramer, F.J., 2022. Modulation of inflammatory responses by a non-invasive physical plasma jet during gingival wound healing. Cells 11 (17), 2740. https://doi.org/10.3390/cells11172740.

Eislmayr, K., Bestehorn, A., Morelli, L., Borroni, M., Vande Walle, L., Lamkanfi, M., Kovarik, P., 2022. Nonredundancy of IL-1a and IL-1b is defined by distinct regulation of tissues orchestrating resistance versus tolerance to infection. Sci. Adv. 8 (9), eabj7293. https://doi.org/10.1126/sciadv.abj7293.

Falanga, V., Isaacs, C., Paquette, D., Downing, G., Kouttab, N., Butmarc, J., Badiavas, E., Hardin-Young, J., 2002. Wounding of bioengineered skin: cellular and molecular aspects after injury. J. Invest. Dermatol. 119 (3), 653–660. https://doi.org/10.1046/j.1523-1747.2002.01865.x.

Falcone, M., De Angelis, B., Pea, F., Scalise, A., Stefani, S., Tasinato, R., Zanetti, O., Dalla Paola, L., 2021. Challenges in the management of chronic wound infections. J. Glob. Antimicrob. Resist. 26, 140–147. https://doi.org/10.1016/j.jgar.2021.05.010.

Feng, W., Wang, Z., 2023. Tailoring the swelling-shrinkable behavior of hydrogels for biomedical applications. Adv Sci (Weinh). 10 (28), e2303326. https://doi.org/10.1002/advs.202303326.

Feng, P., Qiu, H., Luo, Y., Hu, J., Cao, Y., Pang, Q., Mou, X., Hou, R., Hou, W., Zhu, Y., 2021. Development of poloxamer hydrogels containing antibacterial guanidine-based polymers for healing of full-thickness skin wound. ACS Biomater Sci. Eng. 7 (9), 4557–4568. https://doi.org/10.1021/acsbiomaterials.1c00600.

Fernandes, K.E., Carter, D.A., 2017. The antifungal activity of lactoferrin and its derived peptides: mechanisms of action and synergy with drugs against fungal pathogens. Front. Microbiol. 8, 2. https://doi.org/10.3389/fmicb.2017.00002.

Giuliano, E., Paolino, D., Fresta, M., Cosco, D., 2018. Drug-loaded biocompatible nanocarriers embedded in poloxamer 407 hydrogels as therapeutic formulations. Medicines (Basel). 6 (1), 7. https://doi.org/10.3390/medicines6010007.

Grosskopf, A.K., Roth, G.A., Smith, A.A.A., Gale, E.C., Hernandez, H.L., Appel, E.A., 2020. Injectable supramolecular polymer-nanoparticle hydrogels enhance human mesenchymal stem cell delivery. Bioeng. Transl. Med. 5 (1), e10147. https://doi.org/10.1002/btm2.10147.

Haddadian, A., Robattorki, F.F., Dibah, H., Soheili, A., Ghanbarzadeh, E., Sartipnia, N., Hajrasouliha, S., Pasban, K., Andalibi, R., Hedayati Ch, M., Azari, A., Chitgarzadeh, A., Bagheri Kashtali, A., Mastali, F., Noorbazargan, H., Mirzaie, A., 2022. Niosomes-loaded selenium nanoparticles as a new approach for enhanced antibacterial, anti-biofilm, and anticancer activities. Sci. Rep. 12 (1), 21938. https://doi.org/10.1038/s41598-022-26400-x.

Hu, C., Zhang, F., Long, L., Kong, Q., Luo, R., Wang, Y., 2020. Dual-responsive injectable hydrogels encapsulating drug-loaded micelles for on-demand antimicrobial activity and accelerated wound healing. J. Control. Release 324, 204–217. https://doi.org/10.1016/j.jconrel.2020.05.010.

Hunter, R.L., Luo, A.Z., Zhang, R., Kozar, R.A., Moore, F.A., 2010. Poloxamer 188 inhibition of ischemia/reperfusion injury: evidence for a novel anti-adhesive mechanism. Ann. Clin. Lab. Sci. 40 (2), 115–125.

Intorasoot, S., Intorasoot, A., Tawteamwong, A., Butr-Indr, B., Phunpae, P., Tharinjaroen, C.S., Wattananandkul, U., Sangboonruang, S., Khantipongse, J., 2022. *In vitro* antimycobacterial activity of human lactoferrin-derived peptide, D-hLF 1-11, against susceptible and drug-resistant *Mycobacterium tuberculosis* and its synergistic effect with rifampicin. Antibiotics (Basel). 11 (12), 1785. https://doi.org/10.3390/antibiotics11121785.

Jacob, S., Nair, A.B., Shah, J., Sreeharsha, N., Gupta, S., Shinu, P., 2021. Emerging role of hydrogels in drug delivery systems, tissue engineering and wound management. Pharmaceutics 13 (3), 357. https://doi.org/10.3390/pharmaceutics13030357.

Janssens, N., Janicot, M., Perera, T., Bakker, A., 2004. Housekeeping genes as internal standards in cancer research. Mol. Diagn. 8 (2), 107–113. https://doi.org/10.1007/BF03260053.

Ju, Z., Li, M., Xu, J., Howell, D.C., Li, Z., Chen, F.E., 2022. Recent development on COX-2 inhibitors as promising anti-inflammatory agents: the past 10 years. Acta Pharm. Sin. B 12 (6), 2790–2807. https://doi.org/10.1016/j.apsb.2022.01.002.

Kapil, S., Sharma, V., 2021. D-Amino acids in antimicrobial peptides: a potential approach to treat and combat antimicrobial resistance. Can. J. Microbiol. 67 (2), 119–137. https://doi.org/10.1139/cjm-2020-0142.

Khan, B., Arbab, A., Khan, S., Fatima, H., Bibi, I., Chowdhry, N.P., Ansari, A.Q., Ursani, A.A., Kumar, S., Hussain, J., Abdullah, S., 2023. Recent progress in thermosensitive hydrogels and their applications in drug delivery area. MedComm-Biomater. Appl. 2 (3), e55. https://doi.org/10.1002/mba2.55.

Kim, H., Kong, W.H., Seong, K.Y., Sung, D.K., Jeong, H., Kim, J.K., Yang, S.Y., Hahn, S.K., 2016. Hyaluronate-epidermal growth factor conjugate for skin wound healing and regeneration. Biomacromolecules 17 (11), 3694–3705. https://doi.org/10.1021/acs.biomac.6b01216.

Lopez-Machado, A., Diaz-Garrido, N., Cano, A., Espina, M., Badia, J., Baldoma, L., Calpena, A.C., Souto, E.B., Garcia, M.L., Sanchez-Lopez, E., 2021. Development of lactoferrin-loaded liposomes for the management of dry eye disease and ocular inflammation. Pharmaceutics 13 (10), 1698. https://doi.org/10.3390/pharmaceutics13101698.

Luo, B., Liang, H., Zhang, S., Qin, X., Liu, X., Liu, W., Zeng, F., Wu, Y., Yang, X., 2015. Novel lactoferrin-conjugated amphiphilic poly(aminoethyl ethylene phosphate)/poly(L-lactide) copolymer nanobubbles for tumor-targeting ultrasonic imaging. Int. J. Nanomedicine 10, 5805–5817. https://doi.org/10.2147/IJN.S83582.

Monika, P., Chandraprabha, M.N., Rangarajan, A., Waiker, P.V., Chidambara Murthy, K. N., 2021. Challenges in healing wound: role of complementary and alternative medicine. Front. Nutr. 8, 791899. https://doi.org/10.3389/fnut.2021.791899.

Morici, P., Florio, W., Rizzato, C., Ghelardi, E., Tavanti, A., Rossolini, G.M., Lupetti, A., 2017. Synergistic activity of synthetic N-terminal peptide of human lactoferrin in combination with various antibiotics against carbapenem-resistant *Klebsiella pneumoniae strains*. Eur. J. Clin. Microbiol. Infect. Dis. 36 (10), 1739–1748. https://doi.org/10.1007/s10096-017-2987-7.

Morici, P., Rizzato, C., Ghelardi, E., Rossolini, G.M., Lupetti, A., 2023. Sensitization of KPC and NDM *Klebsiella pneumoniae* to rifampicin by the human lactoferrin-derived peptide hLF1-11. Microbiol. Spectr. 11 (1), e0276722. https://doi.org/10.1128/spectrum.02767-22.

Mouritzen, M.V., Petkovic, M., Qvist, K., Poulsen, S.S., Alarico, S., Leal, E.C., Dalgaard, L. T., Empadinhas, N., Carvalho, E., Jenssen, H., 2021. Improved diabetic wound healing by LFcinB is associated with relevant changes in the skin immune response and microbiota. Mol. Ther. Methods. Clin. Dev. 20, 726–739. https://doi.org/10.1016/j.omtm.2021.02.008.

Muzzalupo, R., Tavano, L., Cassano, R., Trombino, S., Ferrarelli, T., Picci, N., 2011. A new approach for the evaluation of niosomes as effective transdermal drug delivery systems. Eur. J. Pharm. Biopharm. 79 (1), 28–35. https://doi.org/10.1016/j.ejpb.2011.01.020.

Ohradanova-Repic, A., Prazenicova, R., Gebetsberger, L., Moskalets, T., Skrabana, R., Cehlar, O., Tajti, G., Stockinger, H., Leksa, V., 2023. Time to kill and time to heal: the multifaceted role of lactoferrin and lactoferricin in host defense. Pharmaceutics 15 (4), 1056. https://doi.org/10.3390/pharmaceutics15041056.

Ong, R., Cornish, J., Wen, J., 2023. Nanoparticular and other carriers to deliver lactoferrin for antimicrobial, antibiofilm and bone-regenerating effects: a review. Biometals 36 (3), 709–727. https://doi.org/10.1007/s10534-022-00455-9.

Pouget, C., Dunyach-Remy, C., Magnan, C., Pantel, A., Sotto, A., Lavigne, J.P., 2022. Polymicrobial biofilm organization of *Staphylococcus aureus* and *Pseudomonas aeruginosa* in a chronic wound environment. Int. J. Mol. Sci. 23 (18), 10761. https://doi.org/10.3390/ijms231810761.

Pourjavadi, A., Heydarpour, R., Tehrani, Z.M., 2021. Multi-stimuli-responsive hydrogels and their medical applications. New J. Chem. 45, 15705–15717. https://doi.org/10.1039/D1NJ02260A.

Powers, J.G., Higham, C., Broussard, K., Phillips, T.J., 2016. Wound healing and treating wounds: Chronic wound care and management. J. Am. Acad. Dermatol. 74 (4), 607–625. https://doi.org/10.1016/j.jaad.2015.08.070.

Puca, V., Marulli, R.Z., Grande, R., Vitale, I., Niro, A., Molinaro, G., Prezioso, S., Muraro, R., Di Giovanni, P., 2021. Microbial species isolated from infected wounds and antimicrobial resistance analysis: data emerging from a three-years retrospective study. Antibiotics (Basel). 10 (10), 1162. https://doi.org/10.3390/antibiotics10101162.

Riesco, A., Santos-Buitrago, B., De Las Rivas, J., Knapp, M., Santos-Garcia, G., Talcott, C., 2017. Epidermal growth factor signaling towards proliferation: modeling and logic inference using forward and backward search. Biomed. Res. Int. 2017, 1809513. https://doi.org/10.1155/2017/1809513.

Russo, E., Villa, C., 2019. Poloxamer hydrogels for biomedical applications. Pharmaceutics 11 (12), 671. https://doi.org/10.3390/pharmaceutics11120671.

Sangboonruang, S., Semakul, N., Obeid, M.A., Ruano, M., Kitidee, K., Anukool, U., Pringproa, K., Chantawannakul, P., Ferro, V.A., Tragoolpua, Y., Tragoolpua, K., 2021. Potentiality of melittin-loaded niosomal vesicles against vancomycin-intermediate *Staphylococcus aureus* and Staphylococcal skin infection. Int. J. Nanomedicine 16, 7639–7661. https://doi.org/10.2147/IJN.S325901.

Schilrreff, P., Alexiev, U., 2022. Chronic inflammation in non-healing skin wounds and promising natural bioactive compounds treatment. Int. J. Mol. Sci. 23 (9), 4928. https://doi.org/10.3390/ijms23094928.

Serpico, L., Dello Iacono, S., Cammarano, A., De Stefano, L., 2023. Recent advances in stimuli-responsive hydrogel-based wound dressing. Gels 9 (6), 451. https://doi.org/10.3390/gels9060451.

Serra, R., Grande, R., Butrico, L., Rossi, A., Settimio, U.F., Caroleo, B., Amato, B., Gallelli, L., de Franciscis, S., 2015. Chronic wound infections: the role of *Pseudomonas aeruginosa* and *Staphylococcus aureus*. Expert Rev. Anti Infect. Ther. 13 (5), 605–613. https://doi.org/10.1586/14787210.2015.1023291.

Shi, C., Wang, C., Liu, H., Li, Q., Li, R., Zhang, Y., Liu, Y., Shao, Y., Wang, J., 2020. Selection of appropriate wound dressing for various wounds. Front. Bioeng. Biotechnol. 8, 182. https://doi.org/10.3389/fbioe.2020.00182.

Syed Azhar, S.N.A., Ashari, S.E., Zainuddin, N., Hassan, M., 2022. Nanostructured lipid carriers-hydrogels system for drug delivery: nanohybrid technology perspective. Molecules 27 (1), 289. https://doi.org/10.3390/molecules27010289.

Tao, J., Zhang, Y., Shen, A., Yang, Y., Diao, L., Wang, L., Cai, D., Hu, Y., 2020. Injectable chitosan-based thermosensitive hydrogel/nanoparticle-loaded system for local delivery of vancomycin in the treatment of osteomyelitis. Int. J. Nanomedicine 15, 5855–5871. https://doi.org/10.2147/IJN.S247088.

Ulvatne, H., Haukland, H.H., Samuelsen, O., Kramer, M., Vorland, L.H., 2002. Proteases in *Escherichia coli* and *Staphylococcus aureus* confer reduced susceptibility to lactoferricin B. J. Antimicrob. Chemother. 50 (4), 461–467. https://doi.org/10.1093/jac/dkf156.

Vega Chaparro, S.C., Valencia Salguero, J.T., Martinez Baquero, D.A., Rosas Perez, J.E., 2018. Effect of polyvalence on the antibacterial activity of a synthetic peptide derived from bovine lactoferricin against healthcare-associated infectious pathogens. Biomed. Res. Int. 2018, 5252891. https://doi.org/10.1155/2018/5252891.

Wong, R.W., Guillaud, L., 2004. The role of epidermal growth factor and its receptors in mammalian CNS. Cytokine Growth Factor Rev. 15 (2–3), 147–156. https://doi.org/10.1016/j.cytogfr.2004.01.004.

World Health Organization, 2024. WHO bacterial priority pathogens list, 2024: bacterial pathogens of public health importance to guide research, development and strategies to prevent and control antimicrobial resistance. https://www.who.int/publications/i/item/9789240093461. accessed 20 May 2024.

Xiao, T., Yan, Z., Xiao, S., Xia, Y., 2020. Proinflammatory cytokines regulate epidermal stem cells in wound epithelialization. Stem Cell Res Ther 11 (1), 232. https://doi.org/10.1186/s13287-020-01755-y.

Yang, Y., Zhao, Y., Liu, L., Zhu, W., Jia, S., Li, X., Li, W., 2022. The anti-apoptotic role of COX-2 during in vitro infection of human intestinal cell Line by *Giardia duodenalis* and the potential regulators. Infect. Immun. 90 (3), e0067221. https://doi.org/10.1128/iai.00672-21.

Yoshimura, A., Wakabayashi, Y., Mori, T., 2010. Cellular and molecular basis for the regulation of inflammation by TGF-b. J. Biochem. 147 (6), 781–792. https://doi.org/10.1093/jb/mvq043.

Zhang, K., Shi, X., Lin, X., Yao, C., Shen, L., Feng, Y., 2015. Poloxamer-based in situ hydrogels for controlled delivery of hydrophilic macromolecules after intramuscular injection in rats. Drug Deliv. 22 (3), 375–382. https://doi.org/10.3109/10717544.2014.891272.

Zhang, X., Shu, W., Yu, Q., Qu, W., Wang, Y., Li, R., 2020. Functional biomaterials for treatment of chronic wound. Front. Bioeng. Biotechnol. 8, 516. https://doi.org/10.3389/fbioe.2020.00516.

Zhang, K., Yang, C., Cheng, C., Shi, C., Sun, M., Hu, H., Shi, T., Chen, X., He, X., Zheng, X., Li, M., Shao, D., 2022. Bioactive injectable hydrogel dressings for bacteria-infected diabetic wound healing: a “pull-push” approach. ACS Appl. Mater. Interfaces 14, 26404–26417. https://doi.org/10.1021/acsami.2c04300.

Zhou, W., Duan, Z., Zhao, J., Fu, R., Zhu, C., Fan, D., 2022. Glucose and MMP-9 dual-responsive hydrogel with temperature sensitive self-adaptive shape and controlled drug release accelerates diabetic wound healing. Bioact. Mater. 17, 1–17. https://doi.org/10.1016/j.bioactmat.2022.01.004.